

# Material ablation and plasma plume expansion study from Fe and graphite targets in Ar gas atmosphere

S. Mahmood · R.S. Rawat · S.V. Springham · T.L. Tan ·  
P. Lee

Received: 22 November 2009 / Accepted: 15 June 2010 / Published online: 21 July 2010  
© Springer-Verlag 2010

**Abstract** Study of expansion dynamics of pulsed-laser ablation plasmas from Fe and graphite targets is presented. A 532 nm Q-switched Nd:YAG laser with fluence of  $30 \text{ J cm}^{-2}$  is used to ablate the Fe and graphite targets in various Ar ambient gas pressures. Plasma ablation parameters for the two target materials are estimated using snow-plow and shock-wave models, which show that the laser beam energy deposited to ablated species remains at 70% for both targets at all ambient pressures. The plume splitting was observed, more prominently, for Fe plasma as it moves faster compared to graphite plasma. The difference in plasma plume fronts' speeds for different targets was attributed to the significant difference in mass of the ablated plasma for two targets, as estimated from simulation results.

## 1 Introduction

The expansion dynamics of laser ablation plasma through ambient gas is a complex mechanism [1, 2]. The fundamental processes involved in plasma expansion like; deceleration, shock-wave formation, thermal conduction, diffusion, recombination, and clustering through ambient gas, are not

yet fully understood [1–5]. The initial expansion of the ablated plasma in a background gas atmosphere is almost independent of the filling gas pressure due to the very high plasma expansion pressure. As the plasma plume moves farther from the target, the interaction processes between the ablated debris and the background gas control its expansion dynamics. In the last few decades, with the development of the high power pulsed lasers, extensive work has been done on the dynamics of plasma plumes in vacuum and in ambient gas pressure, during pulsed-laser deposition (PLD) [1–9].

When a pulse of energetic laser strikes the target with fluence in excess of the ablation threshold of the material, chemical bonds are broken and a shower of electrons, neutral atoms, molecules, and ions is generated [1, 2]. This very hot cloud of energetic fragments of the target material propagates towards the substrate, through the background gas, with a high velocity resulting in the formation of strong shock waves. Accordingly, the role of the background gas is crucial to the properties of the deposited thin films and nanostructures.

During pulsed-laser ablation of solid materials, the hot plasma of material species is ejected from the target surface with very high kinetic energy. The temperature of these plasmas can easily reach several hundreds of eV. During the expansion, these species undergo various chemical reactions by themselves and with the ambient gas. The type of the targets also plays an important role in controlling the dynamics of the plume due to the varying absorption coefficient of materials for a particular wavelength of laser pulse.

This paper presents the dynamics of the Fe and graphite plasma plume during their propagation through different Ar ambient gas pressures. The snow-plow and shock-wave models [10, 11] were used to fit the experimental data obtained from fast-gated imaging and to discuss the plume dynamics. The snow-plow model provides a reasonably good

S. Mahmood · R.S. Rawat (✉) · S.V. Springham · T.L. Tan ·  
P. Lee  
NSSE, NIE, Nanyang Technological University,  
Singapore 637616, Republic of Singapore  
e-mail: [rajdeep.rawat@nie.edu.sg](mailto:rajdeep.rawat@nie.edu.sg)

S. Mahmood  
e-mail: [shamahmood65@yahoo.com](mailto:shamahmood65@yahoo.com)

S. Mahmood  
Department of Physics, University of Karachi, Karachi 75270,  
Pakistan

estimate of ablation parameters and has also been used to predict the plume front position, its velocity and kinetic energy. Another main purpose of this paper is to investigate the effect of the background gas pressure and target material on the plasma plume splitting [12–14]. The plume splitting is of great interest because the fast component of the plume splitting may damage the growing film or otherwise affect its microstructure [12].

## 2 Experimental setup

The imaging of the ablated plasma plume was conducted in a pulsed-laser deposition chamber. The deposition chamber was evacuated to  $\sim 5 \times 10^{-6}$  mbar base pressure and filled with Ar gas at pressures of  $2 \times 10^{-4}$ , 2 and 20 mbar. The plasma was produced by ablation of high purity Fe and graphite targets, using a 48 mJ Q-switched Nd:YAG laser (Continuum-Surelite II) at 532 nm, with a pulse width of  $\sim 8$  ns. The laser beam was focused onto the rotating target disc, using a convex lens of 1 m focal length, with a fluence of  $30 \text{ J cm}^{-2}$ . A schematic of the experimental setup used for plume imaging is shown in Fig. 1. The plasma plume images were captured using a fast-gated ICCD camera (PI-MAX, Princeton Instruments, model: 7397-0013). A double convex lens of focal length 5 cm was used to collect the light at the camera entrance. A programmable timing generator (PTG, ST-133, Princeton Instruments) was used to produce a precise time delay with set intervals between the laser pulse and image capturing instant with the desired acquisition time window of 10 ns. The time zero setting and synchronization of the plasma plume was established with the help of a photodiode and a digital oscilloscope (Tektronix

TDS 3034) to monitor the signals from laser pulse and the timing generator.

## 3 Results and discussion

The imaging results of ablation of Fe and graphite targets in background Ar gas pressures of  $2 \times 10^{-4}$ , 2 and 20 mbar are shown in Fig. 2. The change in target material seems to affect the shape of ablated plasma plume. For Fe target, the plasma plume changes from nearly forward directed elongated plume at initial stages to spherical plume in a later stage of the expansion. The two very distinct fluorescent regions (the so-called plume splitting) were observed at 2 mbar operation. Figure 2 clearly shows that at lower pressure ( $2 \times 10^{-4}$ ) there is no splitting and with the increase in argon ambient pressure to a moderate value of 2 mbar a very clear and distinctive plume splitting is observed up to 700 ns and 500 ns for Fe and graphite targets, respectively. The plume splitting was not observed for 20 mbar of ambient gas pressure and the plume splitting is more prominent for Fe plasma than graphite.

The plasma expansion dynamics for graphite target is very different from that of metallic targets of Fe. The slow core plasma does not seem to move forward with time ( $2 \times 10^{-4}$  and 2 mbar) and stays with target all the time and that makes plume splitting very obvious in all images at 2 mbar. At later instants, particularly for high-pressure operation, the Rayleigh–Taylor (RT) instability is seen to form and deform the plasma front [6]. The graphite plasma plume also has greater lateral expansion as opposed to that of the elongated plume of the Fe target.

The position versus time ( $R-t$ ) plots, where  $R$  represents the plasma plume front position at different time  $t$ , from

**Fig. 1** The schematic diagram of the laser plume imaging setup in a pulsed-laser deposition system

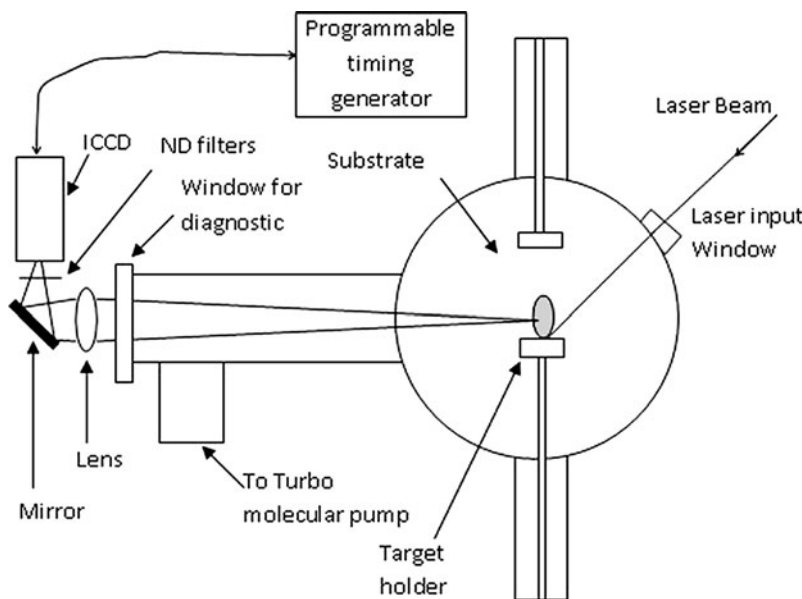
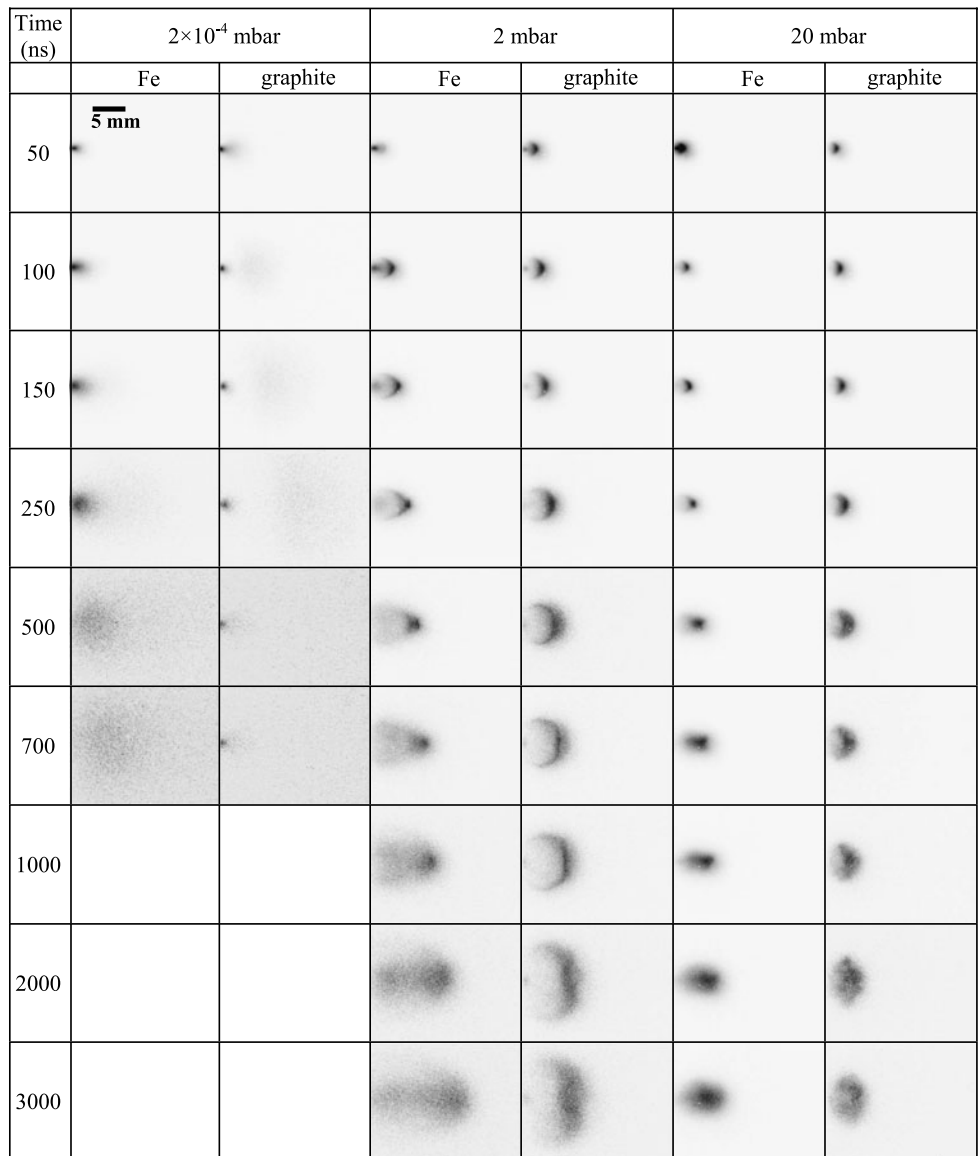


**Fig. 2** The time resolved image sequences of pulsed-laser ablation plasma plumes from Fe and graphite targets expanding in Ar gas background



the experimental data were fitted with the snow-plow and the shock-wave models [10]. In the snow-plow model [10]: when the plasma propagates in vacuum its expansion is free with a constant velocity and its motion is governed by the following equation:

$$F = \frac{d(mv)}{dt} = -P_1 \times A \quad (1)$$

where  $m$  is the mass of the plasma after interaction with the ambient gas,  $v$  is the velocity of the plasma plume front,  $P_1$  is the ambient pressure, and  $A$  is the surface area of the plume that is in contact with the ambient gas. The snow-plow model assumes that plasma expansion is spherical and all the ablated mass is located at the plasma plume front. As plasma expands the ambient gas mass is also added to the

ablated mass, therefore expression for the mass “ $m$ ” can be written as follows:

$$m = m_0 + \rho_1 \frac{2}{3} \pi R^3$$

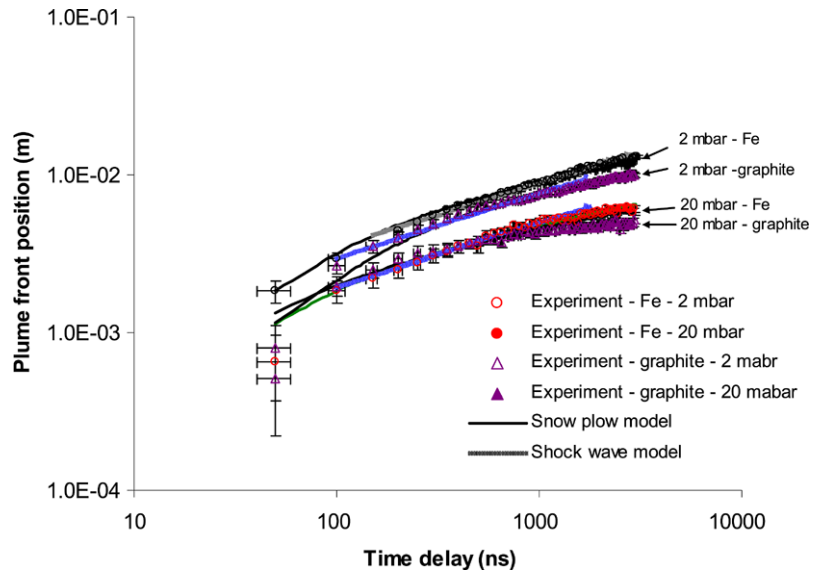
where  $\rho_1$  is the density of the ambient gas and  $R$  is the radius of the expanding spherical plasma plume. Now from (1) we can write:

$$a = \frac{dv}{dt} = -\frac{[P_1 2\pi R^2 - 2\rho_1 \pi R^2 (\frac{dr}{dt})]}{m_0 + \rho_1 (\frac{2}{3}) \pi R^3}$$

The plasma plume front at later time can be estimated using the following equation (where  $R_s$  is the laser spot size):

$$R = R_s + v \Delta t$$

**Fig. 3** Temporal plots ( $R-t$ ) of the experimental data of (a) Fe and (b) graphite ablated plasma fitted with the snow-plow and shock-wave models for different ambient Ar gas pressures



In the shock-wave model [10], we follow the Taylor–Sedov theory [11] where the shock position emerges from the strong point explosion (the shock-wave model describes the explosive release of energy  $E_s$  through a background gas, and neglects viscosity) and is given by

$$R_s = \xi_0 \left( \frac{E_s}{\rho_1} \right)^{\frac{1}{5}} t^{\frac{2}{5}}$$

where  $\xi_0$  is a constant which depends on  $\gamma$ ,  $\gamma$  is the ratio of specific heats of the gas,  $E_s$  is the laser energy coupled to the ablation products, and  $\rho_0$  background gas density, then for the strong shocked.

The typical fitting for 2 and 20 mbar for Fe and graphite targets is shown in Fig. 3. At 2 mbar: (i) the snow-plow model fits the experimental data for the entire duration of imaging for Fe plasma and from about 100 ns to  $\sim 3 \mu\text{s}$  for graphite plasma, whereas (ii) the shock-wave model fits well for the duration of  $\sim 0.2$  to  $\sim 3 \mu\text{s}$  for Fe plasma and  $\sim 0.15$  to  $\sim 1 \mu\text{s}$  for graphite plasma. At 20 mbar, the snow-plow model also fits well (almost as good as it fits for 2 mbar) for Fe plasma, whereas the shock-wave model fits well for the duration of  $\sim 0.1$  to  $\sim 1.3 \mu\text{s}$  for Fe plasma and  $\sim 0.1$  to  $\sim 0.6 \mu\text{s}$  for graphite plasma. For both the pressures, the shock-wave model fits for a short duration as compared to the snow-plow model. This is due to: (i) easy interpenetration of the ablated species and the gas atoms at relatively lower ambient pressure causing shock to start later, and (ii) earlier equilibration of the ambient gas pressure by plumes' internal pressure at high ambient pressure.

Table 1 shows the comparison of the experimental and the calculated ablation and expansion parameter values. The fitting shows that the fraction of input laser energy deposited to the ablated species is about 70%. The snow-plow model

shows that the density of the ambient gas atoms which interacts with the ablated species is different from the filling gas. The initial size of the plasma at time zero (the time instant of the laser pulse peak at the target) as estimated from the snow-plow model is the same as the experimentally measured value,  $R_s$ . The estimated density of the ambient gas, through simulation fitting, is found to be less than the actual filling ambient gas density,  $\rho_1$ . It was about 14% to 22% of actual filling density at 2 mbar and 50% to 80% at 20 mbar, which is because the estimated ambient gas density through simulation actually represents the gas density that interacts with the plasma plume. It therefore increases with the increase in gas pressure as there will be larger number of interactions between the ablated species and the ambient gas atoms for higher filling gas pressures. The calculated amount of ablated mass is greater for the graphite, by 20% and 10% at 2 and 20 mbar respectively, as compared to the measured value,  $m_0$ . This may be due to different physical properties of Fe and graphite, which leads to different ablation efficiency.

Figure 2 shows that the plume of graphite plasma moves slower, in the forward direction, as compared to the Fe plume. It may be noticed from Table 1 that  $E_s$ , the laser energy deposited to the ablated material, is similar for both the filling gas pressures for both the targets. Since the ablated mass of graphite is higher but the energy deposited to this ablated material is the same (as that for Fe ablated plasma of less mass), the ablated plasma plume from graphite will move with lower speed, as observed.

#### 4 Conclusion

Fast-gated imaging of the laser ablated Fe and graphite plasma plumes was carried out for three different ambient

**Table 1** Comparison of experimental and the calculated values of ablation and expansion parameter

Experimental values	Snow plow				Shock wave			
	Fe		graphite		Fe		graphite	
	2 mbar	20 mbar	2 mbar	20 mbar	2 mbar	20 mbar	2 mbar	20 mbar
$E_s$ (J)	$E_0 = 4.75 \times 10^{-2}$	$3.33 \times 10^{-2}$ (70%)	$3.33 \times 10^{-2}$ (70%)	$3.33 \times 10^{-2}$ (70%)	$3.33 \times 10^{-2}$ (70%)	$3.33 \times 10^{-2}$ (70%)	$3.33 \times 10^{-2}$ (70%)	$3.33 \times 10^{-2}$ (70%)
$m_0$ (kg)	$6 \times 10^{-11}$ (Fe) $2.96 \times 10^{-11}$ (graphite)	$6 \times 10^{-11}$ (100%)	$6 \times 10^{-11}$ (100%)	$3.33 \times 10^{-11}$ (120%)	$3.26 \times 10^{-11}$ (110%)	–	–	–
$R_s$ (m)	$225 \times 10^{-6}$ (100%)	$225 \times 10^{-6}$ (100%)	$225 \times 10^{-6}$ (100%)	$225 \times 10^{-6}$ (100%)	$225 \times 10^{-6}$ (100%)	–	–	–
$\rho_l$ ( $\text{kg m}^{-3}$ )	$3.23 \times 10^{-3}$ (2 mbar) $3.23 \times 10^{-2}$ (20 mbar)	$4.52 \times 10^{-4}$	$6.46 \times 10^{-3}$	$7.11 \times 10^{-4}$	$6.46 \times 10^{-3}$	$1.62 \times 10^{-3}$	$1.94 \times 10^{-2}$	$2.58 \times 10^{-3}$ $2.58 \times 10^{-2}$

$E_s$  Laser energy deposited to ablated plasma in model

$E_0$  Experimental value of laser energy at the target

$m_0$  Experimentally measured by collecting ablated material for large number of laser pulses [10]

$R_s$  Experimentally measured laser spot size

$\rho_l$  Density of argon estimated from filling gas pressures which were measured experimentally

pressures of  $2 \times 10^{-4}$ , 2, and 20 mbar of Ar gas to investigate the ablation parameters and expansion dynamics. Some interesting features observed are: initial expansion at  $\sim 50$  ns shows forward directed plume at  $2 \times 10^{-4}$  mbar of ambient pressure, plume splitting at 2 mbar of Ar ambient gas pressure, and plume confinement at 20 mbar of Ar ambient gas pressure. The fitting of calculated values to the experimental data reveals that the fraction of input laser energy deposited to the ablated species is about 70%, for both targets at all ambient gas pressures. The snow-plow model shows that the density of the ambient gas atoms which interact with the ablated species is different from the filling gas. The calculated density of the ambient gas varies from 14% to 22% at 2 mbar and increases to 50% to 80% at 20 mbar of the actual filling gas density. This increase in calculated value of the ambient gas is reasonable because there will be a larger number of interactions between the ablated species and the ambient gas atoms for higher filling gas pressure. The slower speed of graphite plume, as compared to that of Fe plume, was explained using simulated results; according to which the laser energy coupled to ablated graphite plasma is the same as that of Fe plasma but the mass of ablated graphite is higher.

**Acknowledgements** One of the authors (SM) is grateful to the National Institute of Education, Nanyang Technological University Singapore, for providing the research scholarship.

## References

1. R. Eason, *Pulsed Laser Deposition of Thin Films: Application-Led Growth of Functional Materials* (Wiley, New York, 2007)
2. D.B. Chrisey, G.K. Hubler (eds.), *Pulsed Laser Deposition of Thin Films* (Wiley, New York, 1994)
3. D.B. Geohegan, A.A. Puretzky, Appl. Phys. Lett. **67**, 197–199 (1995)
4. S. Amoruso, B. Toftmann, J. Schou, Phys. Rev. E **69**, 056403 (2004)
5. H.C. Le, D.E. Zeitoun, J.D. Parisse, M. Sentis, W. Marine, Phys. Rev. E **62**, 4152–4161 (2000)
6. S.S. Harilal, C.V. Bindhu, M.S. Tillack, F. Najmabadi, A.C. Gaeris, J. Appl. Phys. **93**, 2380–2388 (2003)
7. R.K. Singh, J. Narayan, Phys. Rev. B **41**, 8843–8859 (1990)
8. A.K. Sharma, R.K. Thareja, Appl. Phys. Lett. **84**, 4490–4492 (2004)
9. P.E. Dyer, A. Issa, P.H. Key, Appl. Phys. Lett. **57**, 186–188 (1990)
10. S. Mahmood, R.S. Rawat, M. Zakaullah, J.J. Lin, S.V. Springham, T.L. Tan, P. Lee, J. Phys., D. Appl. Phys. **42**, 135504 (2009)
11. D.A. Freiwald, R.A. Axford, J. Appl. Phys. **46**, 1171 (1975)
12. R.F. Wood, K.R. Chen, J.N. Leboeuf, A.A. Puretzky, D.B. Geohegan, Phys. Rev. Lett. **79**, 1571 (1997)
13. S.S. Harilal, C.V. Bindhu, M.S. Tillack, F. Najmabadi, A.C. Gaeris, J. Phys., D. Appl. Phys. **35**, 2935 (2002)
14. R.F. Wood, J.N. Leboeuf, K.R. Chen, D.B. Geohegan, A.A. Puretzky, Appl. Surf. Sci. **127–129**, 151 (1998)